Quantitative Structural Characterization of Catalytically Active TiO_2 Nanoparticles

Soham Banerjee,† Amirali Zangiabadi,† Akbar Mahdavi-Shakib,‡ Samra Husremovic,¶ Brian G. Frederick,‡ Katayun Barmak,† Rachel Narehood Austin,¶ and Simon J. L. Billinge*,§

†*Department of Applied Physics and Applied Mathematics, Columbia University, New York, NY 10027*

‡*Department of Chemistry, University of Maine, Orono, ME 04469*

¶*Department of Chemistry, Barnard College, Columbia University, New York, NY 10027*

§*Department of Applied Physics and Applied Mathematics, Columbia University, New York, NY 10027*

Condensed Matter Physics and Materials Science Department, Brookhaven National Laboratory, Upton, NY 11973

E-mail: sb2896@columbia.edu

Abstract

This work uses multiple characterization techniques to show conclusively that the pyrogenic TiO_2 photocatalysts, P90 and P25, are made of discrete rutile and anatase nanoparticles and are not composed of a core of anatase with a rutile shell as some studies have posited. Atomic pair distribution (PDF) analysis of P90 demonstrates that the technique is capable of detecting and quantifying minority phases and particle morphology in heterogeneous titania mixtures, with important implications for further studies of shape-controlled nanoparticles with well-defined surface facets.

Keywords

Pair distribution function, nanoparticles, TiO_2, titania, P25, P90, rutile, anatase, morphology, PDF

Introduction

Titania-based materials find widespread uses as photocatalysts, catalysts, solar cells, and biocompatible implants. Their utility depends on a combination of surface, electronic, and bulk structural properties. Our group has been interested in characterizing the properties of nanoparticulate TiO_2 in order to rationally design catalysts for a range of applications.

P90 and P25 are commercial pyrogenic titania nanoparticles (NPs) that contain a mixture of rutile and anatase phases. They are synthesized from vaporized $TiCl_4$ at temperatures between 1000 and 2400 °C, a process referred to as pyrogenesis or fuming. Per the manufacturer, the resulting TiO_2 NPs are 85-90 % anatase by weight, with the rest rutile. The particles are tightly bound to other particles to form aggregates, which enable the material to be distributed as powder or granulates. Numerous researchers have noted that pyrogenic TiO_2 have properties that are quite different from the properties of either anatase or rutile. Hurum *et al.*[1] suggests that P25 contains unusually small rutile crystallites "interwoven" with anatase crystallites, and that this interwoven connection facilitates rapid transfer of electrons from rutile to anatase. Rutile is therefore able to serve as an antenna or photosensitizer to extend the effective anatase band gap to longer wavelengths.

We have recently shown that pyrogenic TiO_2 outperforms other forms of TiO_2 in Ru/TiO_2 catalysts used to hydrodeoxygenate phenol, and much more closely resembles the properties of rutile titania than anatase titania, despite being mostly anatase.[2] Earlier work speculated that P25 might contain particles with a core of anatase overlaid with a shell of rutile,[3] a structure that would be consistent with the catalytic results we obtained. While more recent papers refute the core/shell characterization, a careful review of the literature points to lingering controversy over the structure of pyrogenic TiO_2 and the need for additional characterizations.[4,5]

In this work, we present the first detailed PDF analysis of P90 and P25, supported by x-ray diffraction (XRD) and transmission electron microscopy (TEM) measurements and referenced to recent diffuse reflectance infrared Fourier transform spectroscopy (DRIFTS) and density functional theory (DFT) calculations[6] on the same materials. This shows the importance of structural and morphological characteristics to the properties of the pyrogenic titania. PDF techniques yield complementary information to conventional XRD and TEM such as quantifying the morphology and faceting of the titania nanoparticles in these samples. Our quantitative full profile refinements of the PDF data yield more reliable structural parameters than the single peak phase quantification and Scherrer analyses or lab source Rietveld methods in the current literature.[7–12] By careful benchmarking and model validation we demonstrate that PDF can be used to extract accurate, sample-average information about the crystallographic phases in these nanoparticle mixtures and, furthermore, the nature of their highly faceted morphologies. This lays the ground work for future studies on the relationships between atomic structure, shape, and reactivity.

Experimental Section

Materials

TiO_2 P25 (Evonik), TiO_2 P90 (Evonik), TiO_2 rutile (US Research Nanomaterials), TiO_2 anatase (Sigma Aldrich), were all purchased from their respective manufacturers. 200 mesh Cu TEM grids and silicon nitride grids were purchased from Ted Pella Inc. (Redding, CA). A 90% anatase, 10% rutile mixture was prepared by physically mixing pure anatase and rutile by weight %.

X-Ray diffraction (XRD)

XRD experiments were used to identify the phases present in the powders. These experiments were carried out at the Shared Materials Characterization Laboratory (SMCL) of the Columbia University Nanoinitiative (CNI) at Columbia University using the PANalytical Xpert3 theta-theta Powder x-ray diffraction (XRD) instrument equipped with Cu Kα radiation. The operating voltage was 45 kV and the current 40 mA. The experiments were conducted in the Bragg-Brentano geometry and a zero-background quartz holder was used to minimize the background signal and eliminate reflections from the holder. The two-theta angular range for the scans was 20-100°. The scan step size was 0.1° and the dwell time 1 second per step. For the incident beam, a 15 mm mask and 0.5° divergence and 1° antiscatter slits were employed. For the diffracted beam, the 0.5° antiscatter slit was used. The powder samples were mixed with 2-propanol to allow for ease of placement in the sample holder.

Transmission Electron Microscopy (TEM)

Conventional and high-resolution TEM were performed at the Columbia Nano Initiative (CNI) electron microscopy facilities using an FEI Talos F200X transmission/scanning transmission microscope. The analyzed catalysts were mixed with a minimal amount of 2-propanol and the mixture was suspended on either a lacey carbon film, a Cu grid, or a silicon nitride membrane grid with a membrane thickness of 50 nm, frame width of 50 μm and nine 0.1 mm x 0.1 mm windows. The operating voltage of the FEI Talos was 200 kV. HRTEM imaging was done using the 60 μm objective aperture to include the first diffracting planes of both rutile and anatase ($\{110\}_R$ and $\{101\}_A$) and to achieve higher imaging contrast. Identification of specific TiO_2 particles in the HRTEM image was done by filtering the respective atomic plane periodicity of each phase in fast Fourier transforms (FFT) of the images. Selected area electron diffraction patterns were used to determine the phases present in larger populations of particles compared with the HRTEM images. It was seen that prolonged exposure to the electron beam resulted in amorphization of the particles, and, therefore, in the results presented here, care was taken to minimize the imaging time. Additionally, it was found that the carbon layer in the holey carbon grids was not fully amorphous, making it difficult to unambiguously distinguish the particles from the supporting carbon layer. As a result, the silicon nitride membrane grids were used when there was a need for obtaining the clearest images of the particles.

PDF

Total scattering x-ray measurements were done at the National Synchrotron Light Source II (XPD, 28-ID-2), Brookhaven National Laboratory. Five nanocrystalline TiO_2 samples were measured: anatase, rutile, P90, P25, and a physical mixture containing 90% anatase + 10% rutile by weight fraction. Powder samples were sealed in polyimide capillaries and diffraction patterns were collected at room temperature using the rapid acquisition PDF geometry[13] with an x-ray energy of 67.57 keV ($\lambda = 0.1835$ Å) using a large-area 2D Perkin Elmer detector. The detector was mounted with a sample-to-detector distance of 204.54 mm. The experimental geometry, 2θ range, and detector misorientations were calibrated by measuring a crystalline nickel powder directly prior to the titania nanocrystals, with the experimental geometry parameters refined using the Fit2D program.[14] Standardized corrections were made to the data to obtain the total scattering structure function, $F(Q)$, which was then Fourier transformed to obtain the PDF, using PDFgetX3[15] within xPDFsuite.[16] The maximum range of data used in the Fourier transform (Q_{max}, where $Q = 4\pi \sin\theta/\lambda$ is the magnitude of the momentum transfer on scattering) was chosen to be 20.0 Å^{-1} to give the best tradeoff between statistical noise and real-space resolution.

Though larger Q-ranges were accessible for four of the samples, P90, measured during the same beamtime, had considerably more diffuse scattering at high-Q. Masks were created to remove outlier pixels and to optimize the Q-ranges as much as possible using an automasking procedure[17] and applied to the images before azimuthal integration in PYFAI.[18] For consistency, all five PDFs were transformed with the same settings. See Fig. S6 in the Supporting

Info for a comparison of the Bragg scattering data and $F(Q)$.

PDF structure refinements of pure and mixed TiO_2 samples were first carried out using PDFGUI.[19] The structure models used were rutile (SG: $P4_2/mnm$) and anatase (SG: $I4_1/amd$) as shown in Figure 1 (a, b). The rutile unit cell contains two TiO_2 units and anatase contains four units, but is less dense than rutile, and the TiO_6 octahedra are more distorted. Structure models were obtained from published crystal structures of bulk anatase and rutile.[20,21] For rutile (SG: $P4_2/mnm$), O is at the $2a$ $(0, 0, 0)$ site and Ti at $4f$ $(0.306, 0.306, 0)$. In anatase (SG: $I4_1/amd$), O is positioned at $4a$ $(0, 0, 0)$ and Ti at $8e$ $(0, 0, 0.208)$. To account for the finite size of nanocrystalline TiO_2 particles/crystallites, the PDFs calculated from the crystal structures were attenuated using a characteristic function to approximate the nanoparticle morphology. We refer to this approach as attenuated crystal (AC) modeling. Instrumental parameters were obtained by independently refining a bulk Nickel calibrant and then kept fixed ($Q_{damp} = 0.038$, $Q_{broad} = 0.015$) for all nanoparticle fits. For each TiO_2 phase, $a = b \neq c$ lattice parameters were refined with tetragonal constraints, along with one isotropic atomic displacement parameter (ADP) per element (Ti, O), and a parameter to account for correlated motion effects[22] (δ_1) was also refined.[23] Atomic positions were set to literature values[20,21] and not refined. In the two-phase/mixed AC model, anatase (majority) and rutile (minority) phases were constrained such that the proportion of each phase took values between zero and one.

Discrete structure refinements of faceted anatase models were carried out using the CMI software framework.[24] Unlike the AC modeling approach, here PDFs were calculated from models expressed in cartesian coordinates using the Debye scattering equation,[25] implemented in DIFFPY's DEBYEPDFGENERATOR class under SRFIT. The atomic coordinates were held constant and five parameters were allowed to vary in the PDF refinement: an isotropic expansion coefficient, two isotropic ADPs (one per element), a global scale factor, and δ_1. The discrete anatase models were constructed using a simple cookie-cutting method in VESTA.[26] First the unit cell refined from the AC anatase model was tiled in space to

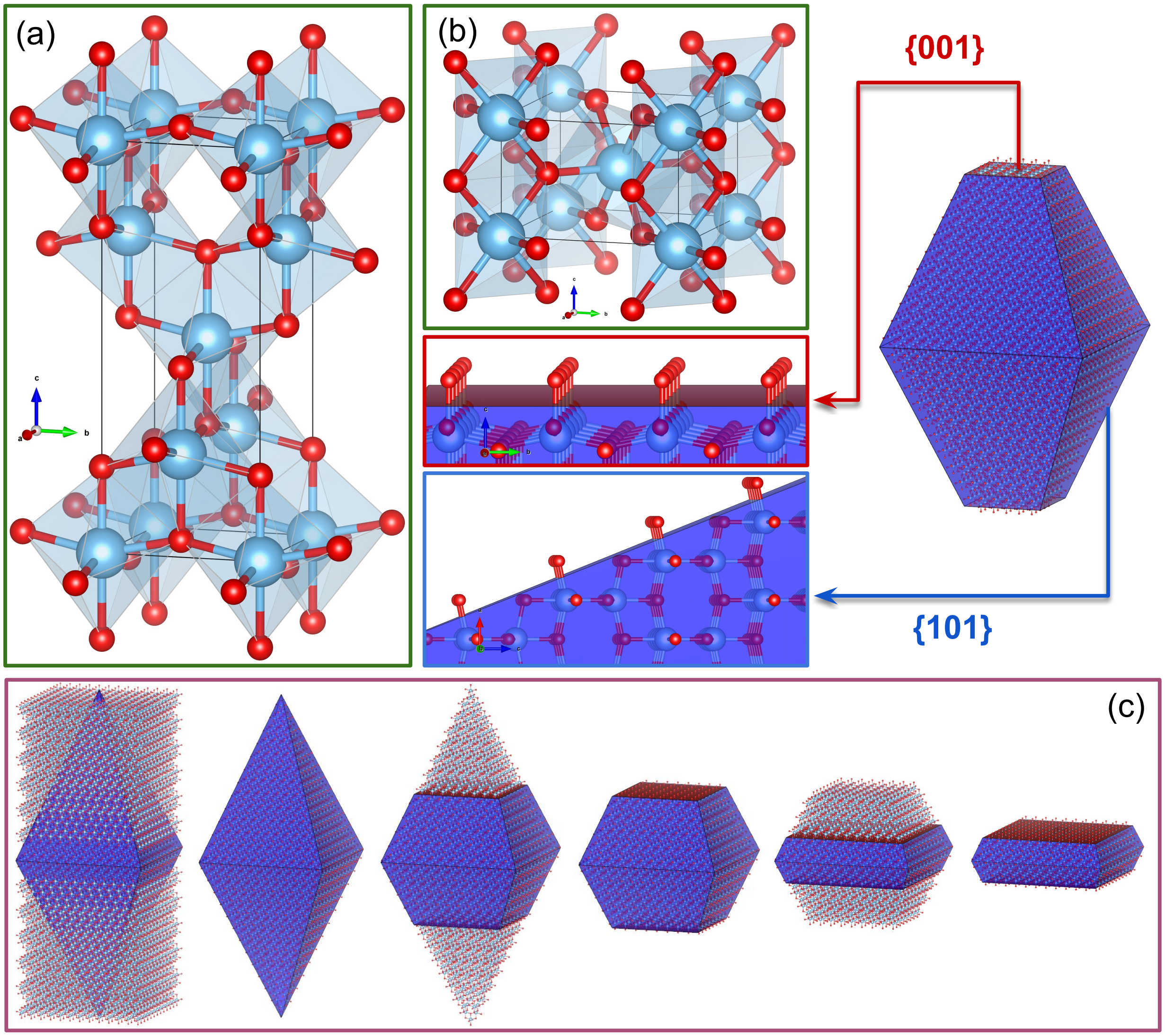

Figure 1: (a): anatase unit cell (b): rutile unit cell. Titanium atoms are shown in blue and xxygen in red. Both tetragonal TiO_2 crystal structures are formed from distorted chains of TiO_6 octahedra (shaded light blue in both unit cells). Right inset: an example of a bipyramidal morphology for anatase with a magnified view of the {001} terminated surface in anatase. The red plane defines the boundary of the surface, where Ti atoms below the plane are undercoordinated with only five nearest O atoms. The corrugated {101} anatase facet with a mixture of five and sixfold coordinated Ti atoms is annotated in blue. (c) An illustration of how shape tuned atomistic models were generated from large anatase supercells.

create a tetragonal supercell where the minimum dimension was made to be $\geq$ the AC refined crystallite diameter. The morphology was then tuned by specifying the Miller indices of anatase surface facets, and generating all symmetry equivalent lattice planes commensurate with the dimensions of the supercell. The surface area ratios between different facets were scaled by changing the relative distances of the facets from the origin of the supercell. The discrete atomic coordinates for each shape were extracted from the supercell by defining cutoff boundaries at the facet limits, illustrated in Figure 1(c). For the large anatase cutouts used in this study, we constrained the number of atoms in each model to be similar (24100±100 atoms) so that the comparisons would be most sensitive to morphological differences. For both AC and discrete structure refinements, the agreement between simulated PDFs and data were quantified by the residual, R_w.[19]

Results

XRD

Figure 2 shows x-ray diffractograms in the angular range of 20-60° for samples of anatase, rutile, P90, P25, and a 90:10 physical mixture of anatase and rutile. The presence of both anatase and rutile in P25, P90 and the physical mixture is clearly evident. The pure TiO_2 samples are indexed and show good agreement to the expected reflections for pure anatase and rutile phases.

TEM

High-resolution transmission electron microscopy (HRTEM) images of P90 and P25 are not consistent with a core/shell model. These images, an example of which is shown in Figure 3 for both P90 and P25, suggest the majority of the particles are pure anatase. Distinct particles of the minority rutile phase, which can be differentiated from anatase by interplanar spacing, are also observed in the images and highlighted in Figure 3. The selected area

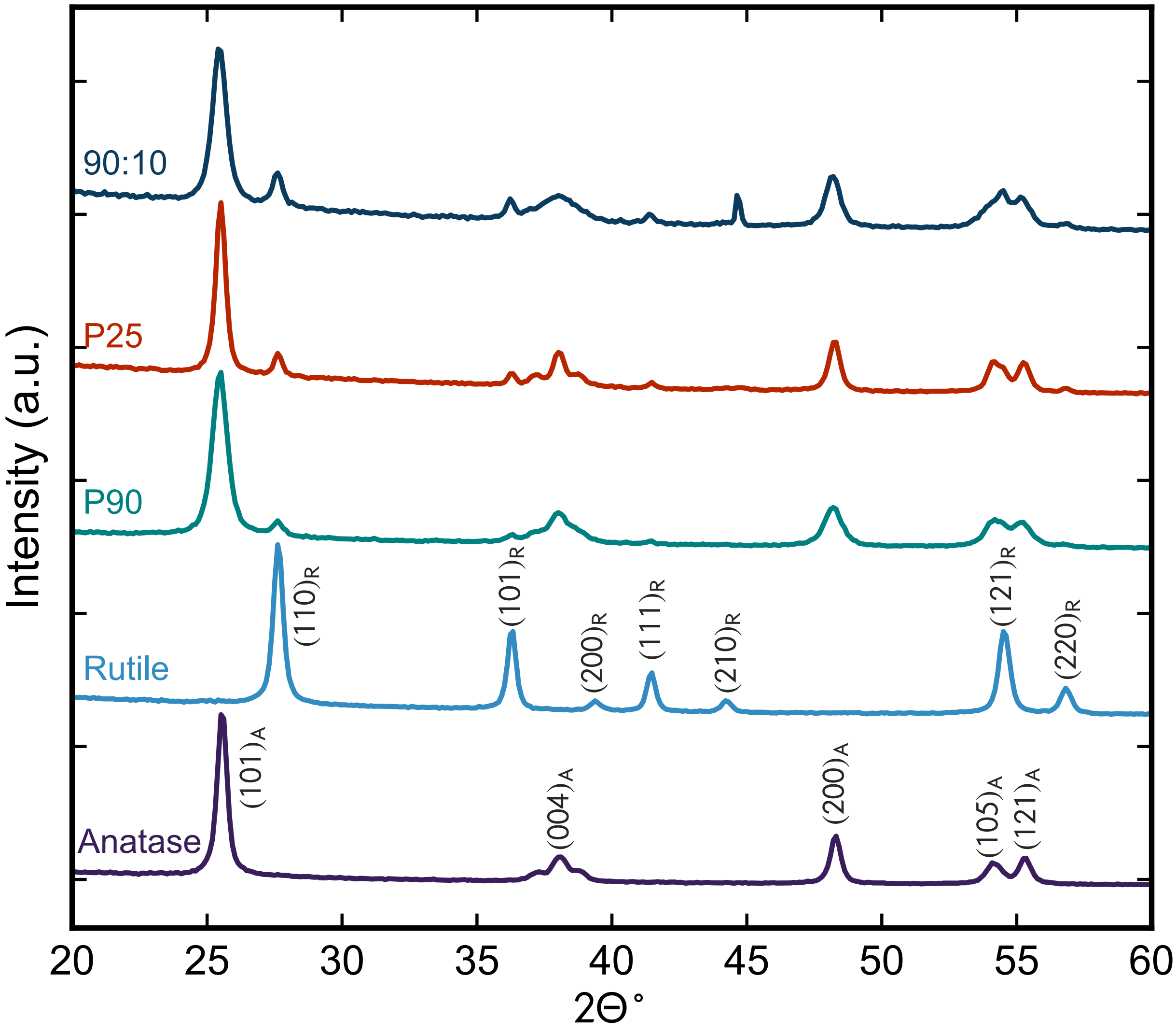

Figure 2: X-ray diffractograms patterns for samples of anatase, rutile, P90, P25, and a physical mixture of 90% anatase and 10% rutile (wt.%). The patterns have been displaced for clarity.

diffraction pattern of P90 and P25 given in Figure 4 also clearly evidences the presence of both anatase and rutile as distinct phases. The diffraction spots for rutile are distinguished from the diffraction spots/rings for anatase, as labeled. The two phases have different crystal structures and thus different interplanar spacings. However, since rutile is the minority phase with a significantly lower phase fraction than anatase in the mixtures, only isolated diffraction spots of rutile are seen in the patterns compared to the more complete diffraction rings of anatase. Representative bright-field transmission electron micrographs of all TiO_2 samples used in this study are provided in the supplemental information and show the sizes and shapes of typical particles (Figure S4 and S5).

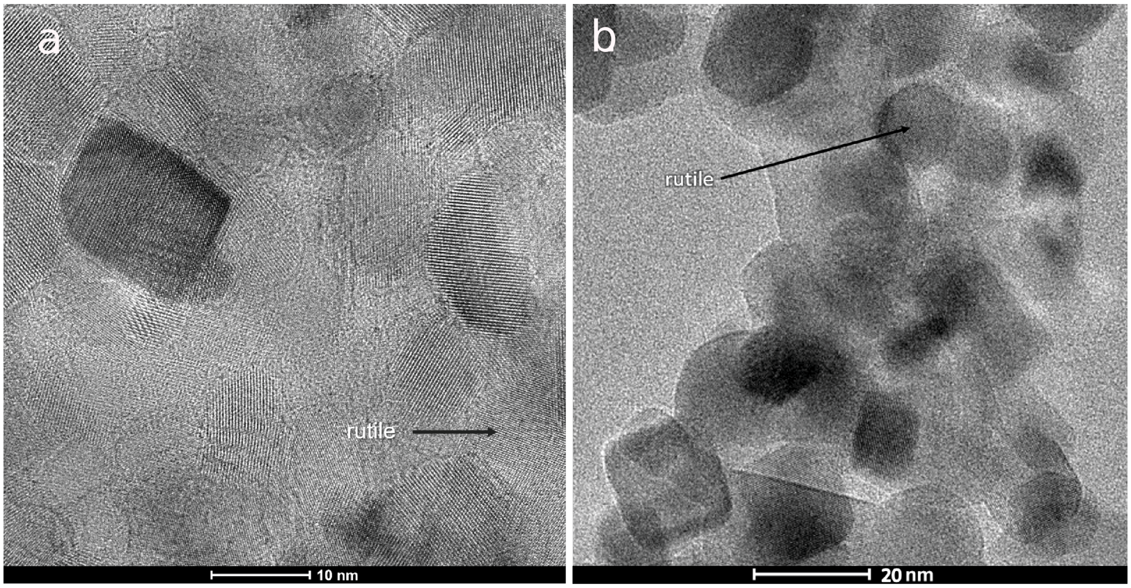

Figure 3: HRTEM images showing individual rutile nanoparticles in P90 (a) and P25 (b) that were identified by interplanar spacing.

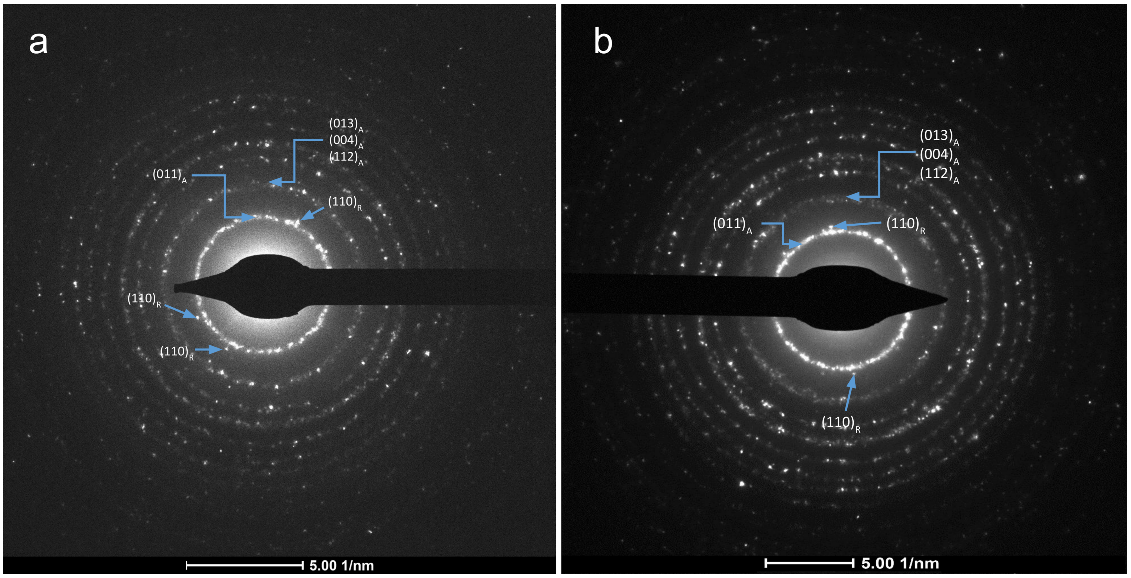

Figure 4: Selected area diffraction of P90 (a) and P25 (b), showing clear evidence of the presence of both anatase and rutile phases. The subscripts A and R denote anatase and rutile, respectively.

PDF

This work presents the first PDF characterization of commercial P90 and P25 nanoparticles. The following analysis was done to accurately quantify the nanocrystalline anatase and rutile phases present in these catalysts, and to assess if there is any evidence of tertiary TiO_2 phases or core/shell phase segregation. PDF is a powerful approach to obtain reliable sample-average structural information from nanomaterials[27–33] and provides insights not readily obtainable by electron microscopy, selected area electron diffraction (SAED) and lab source powder diffraction, all of which have been previously used to characterize pyrogenic TiO_2 nanoparticles.[8–12,34–37]

In order to establish that the PDF is capable of differentiating between the constituent phases of mixed TiO_2 nanomaterials we first analyzed pure anatase and rutile nanoparticles. Single phase refinements of the pure samples, fit to their respective structure models over a wide r-range ($1.5 < r < 60$ Å), are shown in Fig. S1(a-b) and the resulting structural parameters are provided in Table S1. It is clear that the single phase models are in good agreement with the crystallographically distinct nanoparticle structures, evidenced by the small amplitude difference curves and low R_w values (agreement factors) for both samples. We also observe a significant disparity in the average crystallite size between the pure rutile and anatase samples. This can be seen qualitatively by the more rapidly decaying signal intensity (as a function of r) for anatase versus rutile, and quantitatively by the refined spherical particle diameter (SPD) which shows that the pure rutile crystallites are, on average, about twice as large as pure anatase. SPDs, or crystallite sizes, were quantified using the AC modeling approach, commonly applied in PDF analysis.[38] Additional details are included in the PDF Methods section.

Next we measured a physical mixture of anatase and rutile nanoparticles with 90% anatase and 10% rutile by weight to simulate the expected phase fraction of the commercial samples. This was fit initially with a pure anatase model. This results in a quantitatively poorer fit, as evident in Fig. S1(c) and a considerably worse agreement factor compared to the unmixed samples (ΔR_w=+38%), confirming the presence of unfit signal. By refining a two-phase model of anatase and rutile to the physical mixture, we improve the fit to a similar quality as the single phase fit, as shown in Fig. 5(a) and Table 1. In the refinement we allowed the phase fraction of each TiO_2 component to vary, which resulted in a mixing ratio of 89:11 (wt. %) anatase:rutile, consistent with the expected value. This demonstrates the PDF is able to detect and quantify the presence of a minority rutile phase in majority anatase nanocrystalline mixtures.

We then examined the commercial TiO_2 P90 sample. As before we tried to fit it to a pure anatase model. This yielded an $R_w = 0.163$, which is worse than we expect for a good fit as laid out above. On the other hand, the two-phase anatase:rutile model results in an $R_w = 0.129$ that is slightly higher than, but comparable to the best fits to the 90:10 physical mixture, which serves as a method control. The mixing fraction refined to a 87:13 (wt. %) phase mixture of anatase:rutile, which is similar to the manufacturer's claim and earlier non-PDF characterizations.[7,7,35] The results of these refinements are shown in Fig. 5(c) and (d)

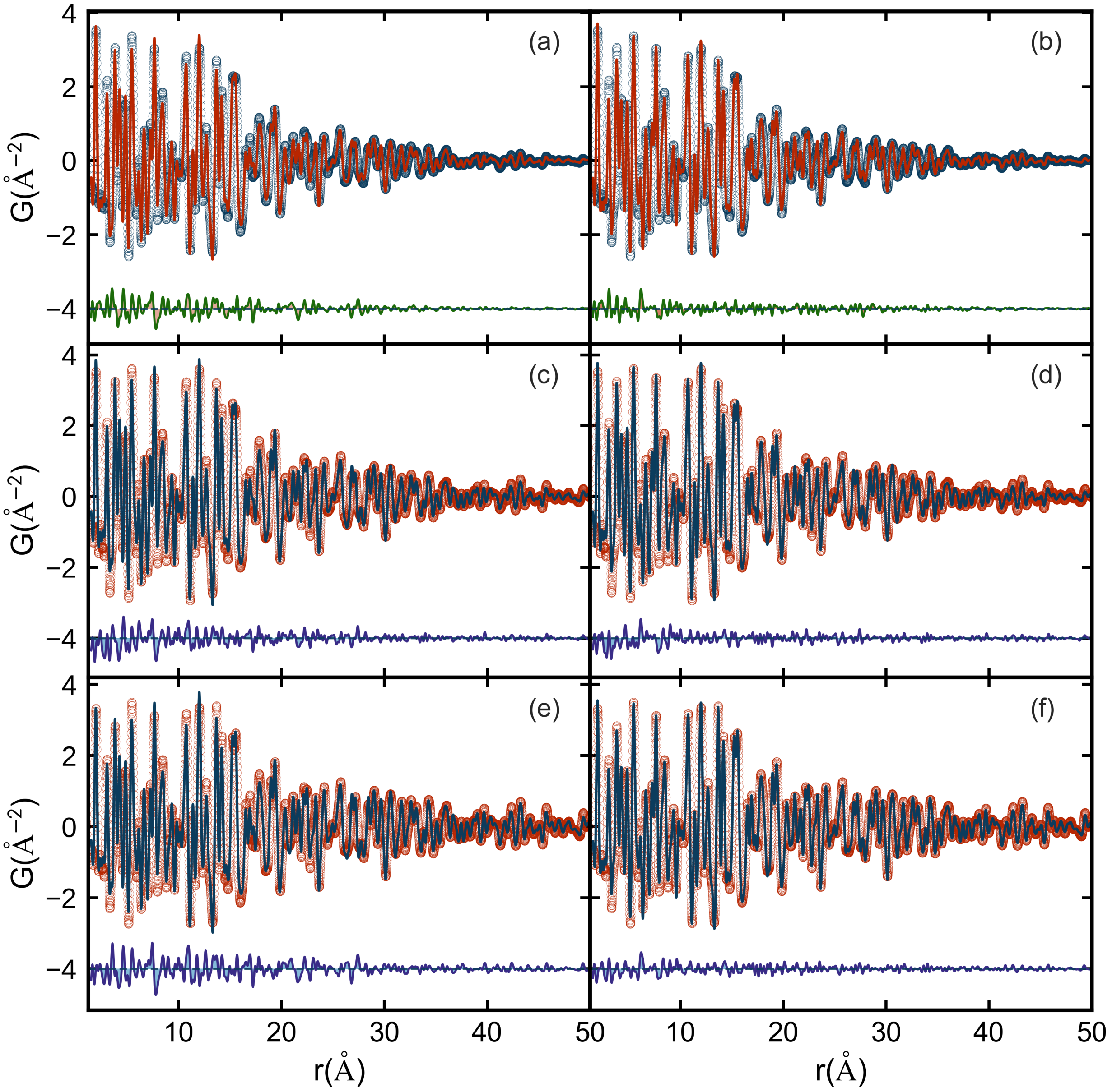

Figure 5: Measured (open symbols) and calculated (solid lines) PDFs of mixed phase, P90 and P25 samples. Difference curves are shown displaced below. Experimental PDFs in the left column are fit with a single phase anatase model for (a) the physical nanoparticle mixture of 90% anatase and 10% rutile (wt.%) (c) P90 and (e) P25. In the right column, experimental PDFs are fit with the mixed phase anatase:rutile model for (b) the physical mixture (d) P90 and (f) P25.

Table 1: Structural parameters extracted from two phase refinements of mixed TiO_2 samples using Anatase (SG: $I4_1/amd$) and Rutile (SG: $P4_2/mnm$) structure models. Lattice parameters for both tetragonal phases are given as $a = b$ and c. U_{iso}: isotropic atomic displacement parameter (ADP) per element and phase. SPD: spherical particle diameter or crystallite size. R_w: agreement factor. See the PDF methods section for additional details.

Sample	P90		P25		$Mix_{90:10}$	
Fit Phase(s)	Anatase	Rutile	Anatase	Rutile	Anatase	Rutile
%	87.47	12.53	84.65	15.35	88.70	11.30
$a = b$ (Å)	3.786	4.589	3.786	4.592	3.783	4.591
c (Å)	9.492	2.963	9.498	2.960	9.498	2.961
Ti U_{iso} (Å^2)	0.005	0.005	0.004	0.005	0.005	0.005
O U_{iso} (Å^2)	0.013	0.029	0.012	0.025	0.015	0.027
SPD (Å)	87.47	66.33	156.35	130.82	65.85	143.42
R_w	0.129		0.108		0.110	

with extracted parameters from mixed phase fits reproduced in Table 1 and single phase fits in Table S1. We also carried out a similar analysis on the commercial P25 sample and found it to be a 85:15 (wt. %) phase mixture of anatase:rutile; fits are shown in Fig. 5(e,f). The agreement to the mixed phase model is as good as the physical mixture, with an $R_w = 0.108$, a clear improvement from the single phase fit shown in Fig. 5(e), further supporting that the two-phase model is appropriate for all three mixed phase TiO_2 samples. Refined parameters for P25 are given in Table 1. Attempts to fit other structural models for the titania gave poorer fits than the physical mixture which strengthens the view that the sample is a mixture of anatase and rutile nanograins.

We looked closely at the refinements of the physical mixture and the pyrogenic TiO_2 samples to search for any differences. As noted, all of the mixed TiO_2 materials included in this study have similar anatase:rutile phase fractions, with P25 having slightly more rutile, and most other structural parameters are comparable. One structural parameter which does differ significantly between the samples is the relative particle/crystallite size (SPD) of the anatase and rutile components. On average, the anatase particles in the physical mixture are smaller than the anatase and rutile crystallites in P90 and P25. In contrast, while the crystallites are smaller in P90 than they are in P25, for both pyrogenic materials the rutile and anatase crystallites are similar in size. While this result differs from several prior reports, both our PDF and HR-TEM data support this assertion. Refined SPDs are provided for comparison in Table 1. The smaller rutile crystallite size, or the comparable relative size of the anatase and rutile components, may be an important characteristic of pyrogenic titania.

Careful inspection of the fits in Fig. 5 suggests that there are some fluctuations left in the residual. It was recently shown[39] that such, albeit small, residual signals that remain after fitting AC models as we have done here, may contain information about particle morphology and defects. We first confirm that these small signals in the residual have a structural origin. In Fig. 6(a) we have replotted the best-fit difference curves from the AC model refinements from Fig. 5(b,d) directly on top of each other. It is clear that these two difference curves are highly correlated with each other, even though the datasets are from completely different samples, in one case the anatase:rutile physical mixture and in the other case, P90. This implies that these two samples share the same structural modification that is not captured in the attenuated crystal modeling. In Fig. S2 we show that this shared structural modification is also present in P25 and in the residual from a single phase refinement of pure anatase. This is a structural modification that is common to all the anatase containing samples.

To explore the structural origin of the residual feature we picked P90 as our representative dataset to study. In Banerjee *et al.*[39] the residual features in metallic nanoparticle signals were explained by building discrete cluster cores with internal twin interfaces. In the current case, we consider possible discrete models that have been suggested for anatase.[40] A Wulff construction may be used to predict equilibrium shapes of crystals based on the surface energies of different facets.[41] The equilibrium Wulff shape for bulk anatase is a slightly truncated bipyramid, with a majority of the surface ($\sim$94%) containing {101} facets, the most energetically stable anatase surface, and a small percentage of {001} facets. In anatase nanoparticles this morphology may be strongly affected by hydroxylation[42] and tuned by using surfactants that preferentially attach to particular lattice planes at the surface, changing the relative energies of the different surface facets,[43] and allowing for different particle

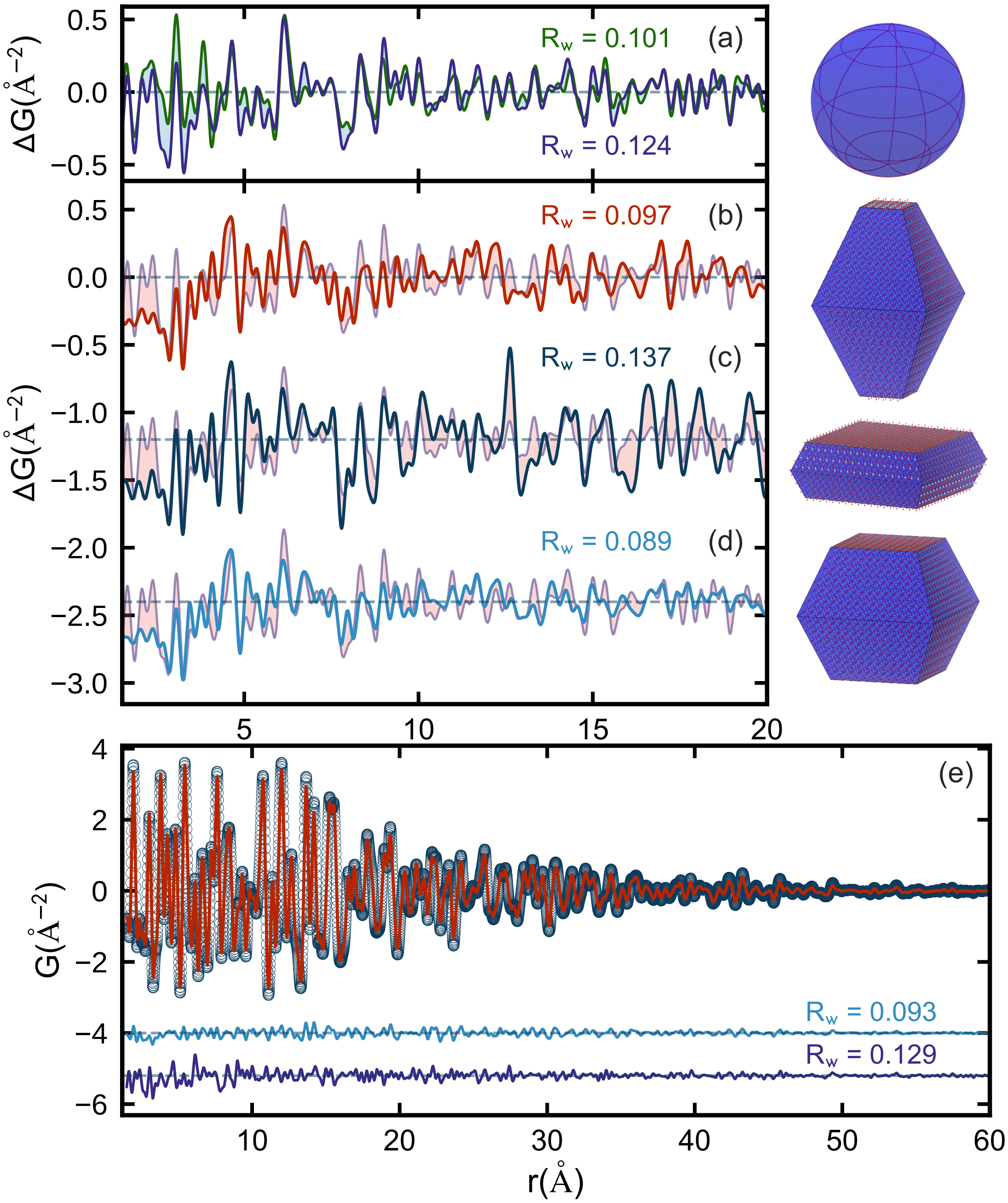

Figure 6: Top panel: difference curves (residuals) from the mixed phase AC model refined to experimental PDFs for P90 (purple) and a physical mixture of 90% anatase and 10% rutile (green). Middle panel: difference curves from discrete anatase models with different percentages of {001} surface facets (a) 5.7% (b) 48.3% and (c) 19.6% fit to the anatase phase in P90. The curves are overlaid with the mixed phase P90 residual in light purple. Right column: the particle morphologies used in the fits. From top to bottom, a spherical approximation used for the AC model followed by the three discrete anatase structure models corresponding to residuals (b-d) in the middle panel. {001} surfaces are shown in red and {101} surfaces in blue. Bottom panel (e): Measured (open circles) and calculated (solid lines) PDFs for P90 refined over the full-r range using the best candidate discrete structure (19.6% {001} faceting). Annotated R_w values are calculated for the range plotted in each panel.

shapes.

We therefore built discrete crystallites with different ratios of surface facet areas to determine if the structural misfit for the mixed TiO_2 samples studied here by PDF could be related to the morphology of the majority anatase phase. Three representative shapes were tested (see Fig. 6). 1) The Wulff model with 5.7% of the anatase surface exposed with {001} facets, 2) a nanoplatelet with 48.3% {001} facets, and 3) an intermediate morphology with 19.6% {001} facets. These were fit to the measured P90 dataset. The PDF from the model accounting for the minority rutile component was also added to the computed anatase model before assessing the agreement, though the parameters of the rutile model were not refined. The resulting residual curves, plotted over a range $1.5 < r < 20$ Å, are shown in Fig. 6 (b), (c) and (d) and the agreement factors, computed over the same r-range, are labeled in the figure. The nanoplatelet shape performs comparably to but slightly worse than the attenuated crystal model. However, there are significant improvements in the agreement for clusters with surfaces containing a much higher percentage of {101} facets, which are the Wulff and intermediate morphologies. The best agreement we obtained was for a particle with ∼20% {001} faceting and 80% {101} facets yielding an $R_w = 0.089$ computed over this low-r range, down from $R_w = 0.124$ for the AC model. This is a significant improvement for the addition of zero refinable variables, which is also evident as qualitatively smaller amplitude oscillations in the residual curve (Fig. 6(d)).

Finally, we selected the best candidate anatase shape with ∼20% {001} faceting and refined this to the raw P90 PDF over the full r-range to $R_{max} = 60$ Å. This refinement resulted in a significant improvement over the AC model over the entire range, with the R_w decreasing from 0.129 to 0.093 (Δ R_w = -32%). The fit also resulted in smaller refined ADPs, particularly for oxygen, with a decrease from 0.013 to 0.009, which alongside lower residuals is often an indication that a model is capturing the correct structure.

Discussion

The work was motivated by a desire to understand why many of the properties of pyrogenic titania are different from the properties of nanoparticulate anatase, despite being mostly anatase. Bickley *et al.* interpreted the presence of Moire fringes in HRTEM data as indicating a rutile core/anatase shell structure for P25.[44] Later work by Datye *et al.* and Ohno *et al.* refuted the core/shell model but both papers left open the possibility that a thin layer of rutile could have escaped detection.[8,11] In this work, we provide evidence from TEM that P90 and P25 contain discrete intermingled particles of anatase and rutile titania. Careful PDF analysis of these materials finds no support for a core/shell structure. In a detailed DRIFTS study of surface hydroxyls coupled to DFT calculations that permitted assignment of bands to specific facets of particular crystal structures, we recently found compelling evidence that P90 and P25 contain surface hydroxyls from both anatase and rutile, again evidence that is inconsistent with a core/shell model.[6]

Shape controlled synthesis of pure anatase nanoparticles with specific ratios of surface facets is a common route towards tailoring their catalytic properties.[40,45] Although this methodology is well-established and previous studies have demonstrated that powder diffraction can be sensitive to changes in anatase morphologies,[33] the connections between surface faceting and catalytic activity in surfactant-free mixed TiO_2 materials, particularly pyrogenic P90/P25, remain unclear. In terms of differentiating pure TiO_2 mixtures from the pyrogenic, commercial samples, the main observation from the PDF analysis is that structurally and morphologically, these samples are rather similar. The primary difference lies in the relative particle sizes between minority and majority TiO_2 phases. In the physical mixture prepared from commercial anatase and commercial rutile, the minority rutile particles are much larger than the anatase particles, wherease in the pyrogenic P90 and P25 samples the anatase and minority rutile particles are comparably sized. These variations in the relative sizes of the anatase and rutile particle components in a sample may influence the differences in activity between the physical mixture and pyrogenic TiO_2 samples. Superior photocatalytic properites due to slower electron-hole pair recombination rates have been attributed to the particle sizes of pyrogenic titania.[1] Our characterization also confirms the close proximity of the rutile and anatase particles in pyrogenic titania. This close proximity, what Hurum described as "interwoven", may facilitate rapid electron transfer from rutile particles to anatase particles and enhance photocatalysis.[1] Recently published DRIFTS data from our lab points to the importance of surface interactions with water in controlling some catalytic features. Pyrogenic titania is not heavily hydroxylated, in contrast to low temperature synthesized anatase, and we think this difference is important for at least some catalytic applications.[2]

This work also highlights the sensitivity of PDF to nanoparticle morphologies, which has been demonstrated in metallic nanoparticles[39] and in pure nanocrystalline anatase TiO_2.[33] Here we calculated PDFs directly using the Debye scattering equation (DSE) for the representative anatase morphologies. This work lays an alternative roadmap for future PDF studies of nanoparticulate TiO_2 from a broad range of applications and synthesis methods[28] that go well beyond typical PDF modeling routines. The discrete anatase cutouts that were tested to investigate particle morphology do not introduce new interatomic distances than those already present in the AC models, so it was somewhat surprising to us that these differences in shape can influence highly constrained PDF refinements so noticeably. The improvements must originate from changes in site multiplicities which differ based on the different coordination environments of surface terminated lattice planes. In the core of the anatase crystallites each Ti atom is sixfold coordinated to O, while $\{101\}$ facets have both six and fivefold coordinated Ti, and $\{001\}$ surfaces contain only undercoordinated Ti atoms with five nearest neighbor oxygen atoms. When these undercoordinated surface atoms contribute significantly relative to the core, as is the case in nanoparticles, they affect the PDF not only at high-r, but locally as well, as we showed here. Such differences would not be captured by the mixed phase AC models, nor any numerical shape approximations.[33,46,47] However, we are confident from this work that the signals in the PDF are robust for determining the particle morphologies in anatase and the modeling approach we lay out here is straightforward.

Conclusion

This work provides a detailed quantitative characterization of the phase composition in commercially important TiO_2 materials, P90 and P25. XRD and PDF data presented here, along with insights from DRIFTS studies,[2] are all consistent with the presence of a small fraction of discrete rutile crystallites and a majority of discrete anatase crystallites. There is no evidence for core/shell particles. The anatase and rutile crystallites are comparable in size in pyrogenic titania. We demonstrate that PDF is sensitive to TiO_2 particle morphology, which has important implications for efforts to understand how electronic and three-dimensional atomic structure determine the chemical and photochemical reactivity of catalysts, and how those properties change during use.[48]

Supporting Information Available

- Single phase refinements of pure and mixed phase TiO_2 NPs, details regarding the faceted atomistic models, additional TEM images, and total scattering data

This material is available free of charge via the Internet at `http://pubs.acs.org/`.

Acknowledgement

Work in the Billinge group was supported by U.S. Department of Energy, Office of Science, Office of Basic Energy Sciences (DOE-BES) under contract No. DE-SC0012704. Work in the Austin and Frederick groups was supported by the National Science Foundation, Division of Chemistry (NSF-CHE), under award number 1565843. Banerjee acknowledges support from the National Defense Science and Engineering Graduate Fellowship (DOD-NDSEG) program. X-ray PDF measurements were conducted on beamline 28-ID-2 of the National Synchrotron Light Source II, a U.S. Department of Energy (DOE) Office of Science User Facility operated for the DOE Office of Science by Brookhaven National Laboratory under Contract No. DE-SC0012704.

References

1. Hurum, D. C.; Agrios, A. G.; Gray, K. A.; Rajh, T.; Thurnauer, M. C. Explaining the Enhanced Photocatalytic Activity of Degussa P25 Mixed-Phase TiO_2 Using EPR. *J. Phys. Chem. B* **2003**, *107*, 4545–4549.

2. Mahdavi-Shakib, A.; Husremovic, S.; Ki, S.; Glynn, J.; Babb, L.; Sempel, J.; Stavrinoudis, I.; Manual Arce Ramos, J.; Nelson, R.; Grabow, L. C. *et al.* Titania surface chemistry and its influence on supported metal catalysts. *Polyhedron.* **2019**, *170*, 41–50.

3. Bickley, R. I.; Gonzalez-Carreno, T.; Lees, J. S.; Palmisano, L.; Tilley, R. J. D. A Structural Investigation of Titanium Dioxide Photocatalysts. *Journal of Solid State Chemistry* **1991**, *92*, 178–190.

4. Mino, L.; Spoto, G.; Bordiga, S.; Zecchina, A. Particles, Morphology, and Surface Properties as Investigated by HRTEM, FTIR, and Periodic DFT Calculations: From Pyrogenic TiO_2 to Nanoanatase. *J. Phys. Chem. C* **2012**, *116*, 17008–17018.

5. Dayte, A. K.; Riegel, G.; Bolton, J. R.; Huang, M.; Prairie, M. R. Microstructural Characterization of a Fumed Titanium Dioxide Photocatalyst. *Journal of Solid State Chemistry* **1995**, *115*, 236–239.

6. Mahdavi-Shakib, A.; Arce-Ramos, J. M.; Austin, R. N.; Schwartz, T. J.; Grabow, L. C.; Frederick, B. G. Frequencies and Thermal Stability of Isolated Surface Hydroxyls on Pyrogenic TiO_2 Nanoparticles. *J. Phys. Chem. C* **2019**, *Submitted.*

7. Mino, L.; Spoto, G.; Bordiga, S.; Zecchina, A. Rutile Surface Properties Beyond the Single Crystal Approach: New Insights from the Experimental Investigation of Different Polycrystalline Samples and Periodic DFT Calculations. *J. Phys. Chem. C* **2013**, *117*, 11186–11196.

8. Ohno, T.; Sarukawa, K.; Tokieda, K.; Matsumura, M. Morphology of a TiO_2 Photocatalyst (Degussa, P-25) Consisting of Anatase and Rutile Crystalline Phases. *Journal of Catalysis* **2001**, *203*, 82–86.

9. Su, R.; Bechstein, R.; Sø, L.; Vang, R. T.; Sillassen, M.; Esbjörnsson, B.; Palmqvist, A.; Besenbacher, F. How the Anatase-to-Rutile Ratio Influences the Photoreactivity of TiO_2. *J. Phys. Chem. C* **2011**, *115*, 24287–24292.

10. Ohtani, B.; Prieto-Mahaney, O. O.; Li, D.; Abe, R. What Is Degussa (Evonik) P25? Crystalline Composition Analysis, Reconstruction from Isolated Pure Particles and Photocatalytic Activity Test. *Journal of Photochemistry and Photobiology A: Chemistry* **2010**, *216*, 179–182.

11. Datye, A. K.; Riegel, G.; Bolton, J. R.; Huang, M.; Prairie, M. R. Microstructural Characterization of a Fumed Titanium Dioxide Photocatalyst. *Journal of Solid State Chemistry* **1995**, *115*, 236–239.

12. Wang, X. H.; Li, J.-G.; Kamiyama, H.; Katada, M.; Ohashi, N.; Moriyoshi, Y.; Ishigaki, T. Pyrogenic Iron(III)-Doped TiO_2 Nanopowders Synthesized in RF Thermal Plasma: Phase Formation, Defect Structure, Band Gap, and Magnetic Properties. *J. Am. Chem. Soc.* **2005**, *127*, 10982–10990.

13. Chupas, P. J.; Qiu, X.; Hanson, J. C.; Lee, P. L.; Grey, C. P.; Billinge, S. J. L. Rapid acquisition pair distribution function analysis (RA-PDF). *J. Appl. Crystallogr.* **2003**, *36*, 1342–1347.

14. Hammersley, A. P.; Svenson, S. O.; Hanfland, M.; Hauserman, D. Two-dimensional detector software: from real detector to idealised image or two-theta scan. *High Pressure Res.* **1996**, *14*, 235–248.

15. Juhás, P.; Davis, T.; Farrow, C. L.; Billinge, S. J. L. PDFgetX3: A rapid and highly automatable program for processing powder diffraction data into total scattering pair distribution functions. *J. Appl. Crystallogr.* **2013**, *46*, 560–566.

16. Yang, X.; Juhás, P.; Farrow, C.; Billinge, S. J. L. xPDFsuite: an end-to-end software solution for high throughput pair distribution function transformation, visualization and analysis. *arXiv* **2015**, 1402.3163.

17. Wright, C. J.; Zhou, X.-D. Computer-Assisted Area Detector Masking. *J Synchrotron Rad* **2017**, *24*, 506–508.

18. Kieffer, J.; Ashiotis, G.; Deschildre, A.; Nawaz, Z.; Wright, J. P.; Karkoulis, D.; Picca, F. E. The fast azimuthal integration Python library: pyFAI. *J. Appl. Crystallogr.* **2015**, *48*, 510–519.

19. Farrow, C. L.; Juhás, P.; Liu, J.; Bryndin, D.; Božin, E. S.; Bloch, J.; Proffen, T.; Billinge, S. J. L. PDFfit2 and PDFgui: Computer programs for studying nanostructure in crystals. *J. Phys: Condens. Mat.* **2007**, *19*, 335219.

20. Horn, M.; Schwerdtfeger, C. F. Refinement of the Structure of Anatase at Several Temperatures. *Z. Für Krist.* **1972**, 273–281.

21. Baur, W. H.; Khan, A. A. Rutile-Type Compounds. IV. SiO_2, GeO_2 and a Comparison with Other Rutile-Type Structures. *Acta Crystallogr. B* **1971**, *27*, 2133–2139.

22. Jeong, I.; Proffen, T.; Mohiuddin-Jacobs, F.; Billinge, S. J. L. Measuring correlated atomic motion using X-ray diffraction. *J. Phys. Chem. A* **1999**, *103*, 921–924.

23. Proffen, T.; Billinge, S. J. L. PDFFIT, a program for full profile structural refinement of the atomic pair distribution function. *J. Appl. Crystallogr.* **1999**, *32*, 572–575.

24. Juhás, P.; Farrow, C. L.; Yang, X.; Knox, K. R.; Billinge, S. J. L. Complex Modeling: a strategy and software program for combining multiple information sources to solve ill-posed structure and nanostructure inverse problems. *Acta Crystallogr. A* **2015**, *71*, 562–568.

25. Debye, P. Dispersion of Röntgen rays. *Annalen der Physik (Berlin, Germany)* **1915**, *351*, 809–823.

26. Momma, K.; Izumi, F. VESTA: A Three-Dimensional Visualization System for Electronic and Structural Analysis. *J. Appl. Crystallogr.* **2008**, *41*, 653–658.

27. Choi, J. J.; Yang, X.; Norman, Z. M.; Billinge, S. J. L.; Owen, J. S. Structure of methylammonium lead iodide on mesoporous titanium dioxide: active material in high performance metal-organic solar cells. *Nano Lett.* **2014**, *14*, 127–133.

28. Nakamura, N.; Terban, M. W.; Billinge, S. J. L.; Jayan, B. R. Unlocking the structure of mixed amorphous-crystalline ceramic oxide films synthesized under low temperature electromagnetic excitation. *J. Mater. Chem. A* **2017**, *5*, 18434–18441.

29. Jensen, K. M. Ø.; Juhás, P.; Tofanelli, M. A.; Heinecke, C. L.; Vaughan, G.; Ackerson, C. J.; Billinge, S. J. L. Polymorphism in magic sized $Au_{144}(SR)_{60}$ clusters. *Nat. Commun.* **2016**, *7*, 11859.

30. Farrow, C. L.; Shi, C.; Juhás, P.; Peng, X.; Billinge, S. J. L. Robust structure and morphology parameters for CdS nanoparticles by combining small angle X-ray scattering and atomic pair distribution function data in a complex modeling framework. *J. Appl. Crystallogr.* **2014**, *47*, 561–565.

31. Zobel, M.; Neder, R. B.; Kimber, S. A. J. Universal solvent restructuring induced by colloidal nanoparticles. *Science* **2015**, *347*, 292–294.

32. Mi, J.-L.; Ø. Jensen, K. M.; Tyrsted, C.; Bremholm, M.; B. Iversen, B. In Situ Total X-Ray Scattering Study of the Formation Mechanism and Structural Defects in Anatase TiO_2 Nanoparticles under Hydrothermal Conditions. *CrystEngComm* **2015**, *17*, 6868–6877.

33. Liu, J.; Olds, D.; Peng, R.; Yu, L.; Foo, G. S.; Qian, S.; Keum, J.; Guiton, B. S.; Wu, Z.; Page, K. Quantitative Analysis of the Morphology of {101} and {001} Faceted Anatase TiO_2 Nanocrystals and Its Implication on Photocatalytic Activity. *Chem. Mater.* **2017**, *29*, 5591–5604.

34. Moiseev, A.; Krichevskaya, M.; Qi, F.; Weber, A. P.; Deubener, J. Analysis of Photocatalytic Performance of Nanostructured Pyrogenic Titanium Dioxide Powders in View of Their Polydispersity and Phase Transition: Critical Anatase Particle Size as a Factor for Suppression of Charge Recombination. *Chem. Eng. J.* **2013**, *228*, 614–621.

35. Moiseev, A.; Qi, F.; Deubener, J.; Weber, A. Photocatalytic Activity of Nanostructured Titanium Dioxide from Diffusion Flame Synthesis. *Chem. Eng. J.* **2011**, *170*, 308–315.

36. Lebedev, V. A.; Kozlov, D. A.; Kolesnik, I. V.; Poluboyarinov, A. S.; Becerikli, A. E.; Grünert, W.; Garshev, A. V. The Amorphous Phase in Titania and Its Influence on Photocatalytic Properties. *Applied Catalysis B: Environmental* **2016**, *195*, 39–47.

37. Pennington, A. M.; Okonmah, A. I.; Munoz, D. T.; Tsilomelekis, G.; Celik, F. E. Changes in Polymorph Composition in P25-TiO_2 during Pretreatment Analyzed by Differential Diffuse Reflectance Spectral Analysis. *J. Phys. Chem. C* **2018**, *122*, 5093–5104.

38. Egami, T.; Billinge, S. J. L. *Underneath the Bragg peaks: structural analysis of complex materials*, 2nd ed.; Elsevier: Amsterdam, 2012.

39. Banerjee, S.; Liu, C.-H.; Lee, J. D.; Kovyakh, A.; Grasmik, V.; Prymak, O.; Koenigsmann, C.; Liu, H.; Wang, L.; Abeykoon, A. M. M. *et al.* Improved Models for Metallic Nanoparticle Cores from Atomic Pair Distribution Function (PDF) Analysis. *J. Phys. Chem. C* **2018**, *122*, 29498–29506.

40. De Angelis, F.; Di Valentin, C.; Fantacci, S.; Vittadini, A.; Selloni, A. Theoretical Studies on Anatase and Less Common TiO_2 Phases: Bulk, Surfaces, and Nanomaterials. *Chem. Rev.* **2014**, *114*, 9708–9753.

41. Lazzeri, M.; Vittadini, A.; Selloni, A. Structure and energetics of stoichiometric TiO_2 anatase surfaces. *Phys. Rev. B* **2001**, *63*, 155409.

42. Arrouvel, C.; Digne, M.; Breysse, M.; Toulhoat, H.; Raybaud, P. Effects of morphology on surface hydroxyl concentration: a DFT comparison of anatase-TiO_2 and γ-alumina catalytic supports. *Journal of Catalysis* **2004**, *222*, 152–166.

43. Gordon, T. R.; Cargnello, M.; Paik, T.; Mangolini, F.; Weber, R. T.; Fornasiero, P.; Murray, C. B. Nonaqueous Synthesis of TiO_2 Nanocrystals Using TiF_4 to Engineer Morphology, Oxygen Vacancy Concentration, and Photocatalytic Activity. *J. Am. Chem. Soc.* **2012**, *134*, 6751–6761.

44. Bickley, R.; Gonzalez-Carrenoa, T.; Lees, J. S.; Palmisano, L.; Tilley, R. D. A structural investigation of titanium dioxide photocatalyst. *Journal of Solid State Chemistry* **1991**, *92*, 178–190.

45. Gong, X.-Q.; Selloni, A. Reactivity of Anatase TiO_2 Nanoparticles: The Role of the Minority (001) Surface. *J. Phys. Chem. B* **2005**, *109*, 19560–19562.

46. Usher, T.-M.; Olds, D.; Liu, J.; Page, K. A Numerical Method for Deriving Shape Functions of Nanoparticles for Pair Distribution Function Refinements. *Acta Crystallogr. Sect. Found. Adv.* **2018**, *74*, 322–331.

47. Olds, D.; Wang, H.-W.; Page, K. *DShaper*: An Approach for Handling Missing Low-Q Data in Pair Distribution Function Analysis of Nanostructured Systems. *J. Appl. Crystallogr.* **2015**, *48*, 1651–1659.

48. Polo-Garzon, F.; Bao, Z.; Zhang, X.; Huang, W.; Wu, Z. Surface Reconstructions of Metal Oxides and the Consequences on Catalytic Chemistry. *ACS Catal.* **2019**, *9*, 5692–5707.